Global optimization for quantum dynamics of few-fermion systems

Xikun Li,[1] Daniel Pęcak,[2] Tomasz Sowiński,[2] Jacob Sherson,[1] and Anne E. B. Nielsen[3,*]
[1]*Department of Physics and Astronomy, Aarhus University, DK-8000 Aarhus C, Denmark*
[2]*Institute of Physics, Polish Academy of Sciences, Aleja Lotnikow 32/46, PL-02668 Warsaw, Poland*
[3]*Max-Planck-Institut für Physik komplexer Systeme, D-01187 Dresden, Germany*

(Received 30 January 2018; published 1 March 2018)

Quantum state preparation is vital to quantum computation and quantum information processing tasks. In adiabatic state preparation, the target state is theoretically obtained with nearly perfect fidelity if the control parameter is tuned slowly enough. As this, however, leads to slow dynamics, it is often desirable to be able to carry out processes more rapidly. In this work, we employ two global optimization methods to estimate the quantum speed limit for few-fermion systems confined in a one-dimensional harmonic trap. Such systems can be produced experimentally in a well-controlled manner. We determine the optimized control fields and achieve a reduction in the ramping time of more than a factor of four compared to linear ramping. We also investigate how robust the fidelity is to small variations of the control fields away from the optimized shapes.

DOI: 10.1103/PhysRevA.97.033602

I. INTRODUCTION

Quantum optimal control is essential to manipulate and engineer complex quantum systems in quantum information processing and quantum computation [1–3]. Operations in experiments are often executed adiabatically to guarantee the transition to the target state with almost-perfect fidelity [4]. The adiabatic process, however, needs to be done slowly, and it is therefore interesting to look for ways to achieve a speedup, which is a topic of the field of quantum optimal control [5,6].

The minimal allowed time for driving such transitions with perfect fidelity is known as the quantum speed limit (QSL) [7,8]. The QSL is a lower bound for the duration in which the quantum system can be completely steered to the target state [8–13]. For durations shorter than the QSL, defects emerge that lead to a drop in fidelity between the target state and the obtained state. The quantum optimal control theory is important to obtain the QSL [14] and has been applied using certain numerical methods in many quantum systems like NMR [15], Bose-Einstein condensates [16–18], and spin chain models [19,20].

Except for a few special cases in which analytical results are available, one has to perform numerical calculations, which are highly nontrivial, due to the high dimensionality of the Hilbert space. Generally, quantum control theory relies on numerical techniques including local optimization algorithms, such as Krotov, GRAPE, and CRAB [21–24], as well as global optimization methods like differential evolution (DE) [25–27] and the covariance matrix adaptation evolution strategy (CMA-ES) [28,29]. In Ref. [30], it is proposed that numerical optimization relies on an appropriate balance between local and global optimization approaches and problem representation. When the quantum system is fully controllable and free of constraints, there are no traps in the form of suboptimal local extrema [31]. In such cases, the local algorithms are preferred, as the computational cost of local optimization methods is lower than that of global ones. When the duration of the process is short or if there are constraints on the control field, local algorithms are often stuck in local suboptimal traps in the quantum control landscape. For the low-dimensional quantum system, the computational cost of multistarting the local optimization algorithms, which gives sufficiently good results, is comparable with that of multistarting the global ones. In Ref. [25], local optimization methods fail to obtain a satisfactory result determined by a certain threshold infidelity for quantum gates, though global optimization methods succeed. The superiority of global optimization methods is also highlighted for the high-dimensional Hamiltonians studied in Ref. [26].

The ultimate goal is to fully control any many-body quantum system. In cold-atom experiments, one can influence the interparticle interaction with an external magnetic field thanks to Feshbach resonances. Due to the adiabatic change of the interaction it is possible to obtain, for example, a highly correlated state known as a Tonks-Girardeau gas starting from the noninteracting state [32–34]. Unfortunately, full control of systems with a large number of particles is very challenging. A possible way to overcome the difficulty of such complex systems is to fully control smaller physical systems and use them to build real many-body systems. A possible candidate to serve this purpose is quantum systems of a few ultracold atoms [35–41]. In two-component mixtures of fermions one can deterministically prepare a system confining a well-established number of atoms with astonishing precision. The properties of few-body ultracold systems were also studied recently theoretically, including energy spectra and density profiles [42–50]. The two different flavors in a mixture of same-mass fermions are realized experimentally by using two different hyperfine states of ultracold lithium ^{6}Li. A natural way to generalize this idea is to change the hyperfine states

*On leave from Department of Physics and Astronomy, Aarhus University, DK-8000 Aarhus C, Denmark.

to two completely different species, for example, lithium and potassium [51,52]. Such an experiment on a two-flavor mixture of lithium and potassium on a many-body scale has been performed [53]. Recently, few-body mass-imbalanced systems were broadly explored theoretically [54–60].

In this paper, we employ two global optimization algorithms, the CMA-ES [28,29] and self-adaptive DE (SaDE) [26,27], to numerically estimate the quantum speed limit for few-fermion mass-imbalanced systems and show the optimized control field for various durations. We consider the fidelity of the final state with respect to the target state as the fitness function to be optimized. As proof of concept we show how to fully control a system of a few fermions and drive it from the noninteracting state to the strongly correlated one.

II. THE MODEL

We consider a two-flavor system of a few ultracold fermions confined in a one-dimensional harmonic trap. Here we assume that the frequencies ω of the harmonic trap are the same for both flavors. Fermions of opposite flavors interact in the ultracold regime via short-range forces modeled by the deltalike potential $U(x-x') = g\delta(x-x')$, where g is the interaction strength [61]. In this approximation fermions of the same type do not interact as a consequence of the Pauli exclusion principle. Fermions of opposite flavors are fundamentally distinguishable and may have the same or different masses (in the following we denote the mass ratio $\mu = m_\uparrow/m_\downarrow$). The Hamiltonian of the mass-imbalanced system reads (see [54–56])

$$\hat{\mathcal{H}} = \sum_{i=1}^{N_\downarrow}\left[-\frac{1}{2}\frac{\partial^2}{\partial x_i^2} + \frac{1}{2}x_i^2\right] + \sum_{j=1}^{N_\uparrow}\left[-\frac{1}{2\mu}\frac{\partial^2}{\partial y_j^2} + \frac{\mu}{2}y_j^2\right] + g\sum_{i,j=1}^{N_\downarrow,N_\uparrow}\delta(x_i - y_j). \quad (1)$$

All quantities are measured in appropriate harmonic oscillator units, i.e., positions are measured in units of $\sqrt{\hbar/(m_\downarrow\omega)}$, time in units of $1/\omega$, energies in $\hbar\omega$, and the interaction strength g is measured in units of $(\hbar^3\omega/m_\downarrow)^{1/2}$.

We employ the exact diagonalization approach to study the dynamics of the few-fermion system (see Ref. [54] for details of the numerical method). The interaction g is controlled experimentally with the help of the magnetic field B, so by changing the magnetic field in time, one can also modify the interaction $g(B(t))$. Thus, it is convenient to treat the interaction strength $g(t)$ as the control field. The many-body spectrum for the system of three fermions is shown in Fig. 1. In this paper, we focus on the transformation from the ground state of the noninteracting Hamiltonian $\hat{\mathcal{H}}(g=0)$ to that of $\hat{\mathcal{H}}(g=10)$, where strong correlations are present. By increasing the interaction adiabatically, one can transfer the noninteracting state $\Psi_{g=0}$ to the interacting one $\Psi_{g=10}$. Note that depending on whether mass imbalance is present in the system, and on the specific configuration, the ground state of the system might be quasidegenerated in the strong interaction limit. For the equal-mass system there is a threefold degeneracy, while for the system 1K-2Li the ground state is not degenerated. For the dynamics considered below, there is no coupling to these additional low-energy states, because they have a different symmetry. The time scale for adiabatic ramping is hence determined not by the energy of these states relative to the

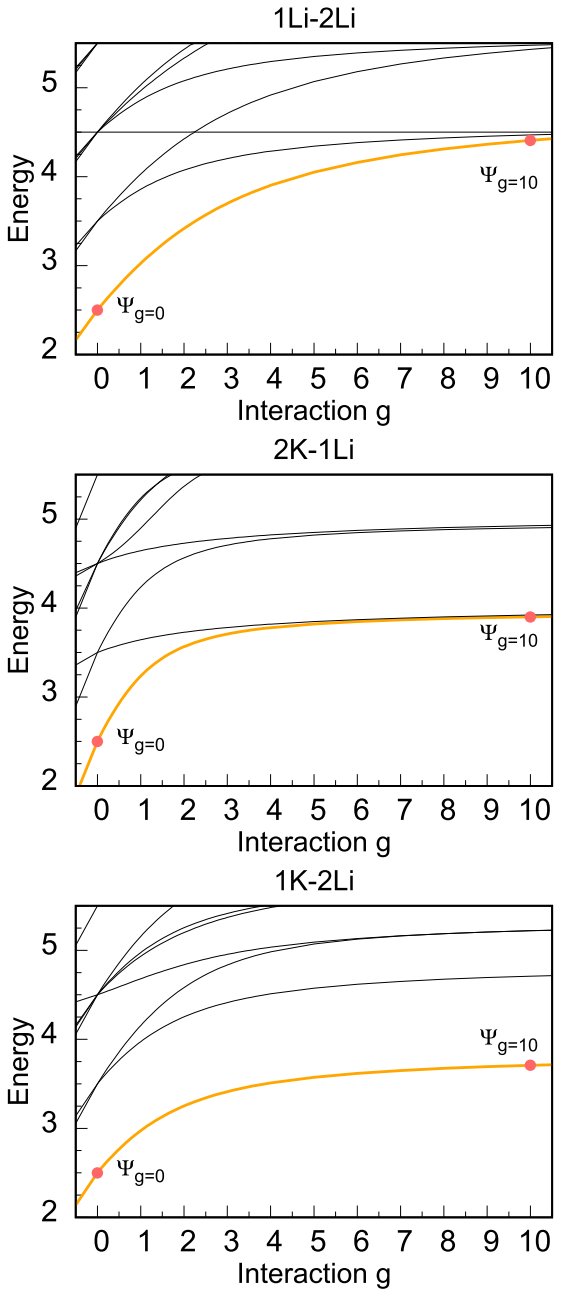

FIG. 1. Energy spectrum of the system of three fermions for three scenarios, namely, 1Li-2Li, 2K-1Li, and 1K-2Li. The thick orange line gives the ground-state energy. The noninteracting ground state $g=0$ and the strongly correlated target state $g=10$ are shown by the red circles. For the 1Li-2Li and the 2K-1Li systems, there are, respectively, two and one other states that have energies close to the ground-state energy in the strong coupling limit. These states do, however, have different symmetries than the ground state, and the population of these states remains 0 throughout the dynamics. The energies and the interaction strengths are measured in units of $\hbar\omega$ and $(\hbar^3\omega/m_\downarrow)^{1/2}$, respectively.

ground state, but by the energy of the higher lying states relative to the ground state.

For a typical quantum control problem, the Hamiltonian depends on a time-dependent control field $\mathcal{H} = \mathcal{H}(g(t))$. We wish to optimize the fidelity as a fitness function,

$$F(g(t),T) = |\langle\Psi_{g=10}|\mathcal{T}\exp\left(-i\int_0^T \mathcal{H}(g(t))dt\right)|\Psi_{g=0}\rangle|^2, \tag{2}$$

with the time evolution driven by the control field $g(t)$, where $\mathcal{T}$ is the time-ordering operator and the duration T is discretized with time-step size $\delta t = 10^{-3}$ for numerical evaluation of the time evolution. It is noteworthy that the most time-consuming part during the numerical calculation is the time evolution, which consists of a long sequence of evaluations of exponentials of large Hamiltonian matrices (see Sec. V). Therefore the maximal number of iterations is set to be 500 for the CMA-ES and SaDE.

To perform this optimization systematically, we choose $g(t)$ to be decomposed into a truncated Fourier basis (CRAB method; see [16] and [21]),

$$g(t) = g_0(t)\left[1 + \frac{1}{\mathcal{N}(t)}\sum_{n=1}^{N_c}(A_n\cos(\omega_n t) + B_n\cos(\omega_n t))\right], \tag{3}$$

where $g_0(t)$ is the initial guess of the control field and $\mathcal{N}(t) = T^2/2t(T-t)$ is a time-dependent function to fix the initial and final control field values at $g(t=0) = 0$ and $g(t=T) = 10$. $\{A_n, B_n\}$ are Fourier coefficients, $\omega_n = 2\pi n(1+r_n)/T$ are "randomized" Fourier harmonics, and $r_n \in [0,1]$. The choice of the cutoff number N_c of the Fourier basis may vary from one case to another: it may depend on the Hamiltonian, the fitness function, and the optimization algorithm. The parameter space (search space) consists of the Fourier coefficients and harmonics $\{A_n, B_n, \omega_n\}$, which can be numerically obtained using an optimization method, e.g., the simplex method, gradient-based strategies, and global optimization algorithms. In this paper, we restrict ourselves to nonnegative interactions $g(t) \geqslant 0$ by simply setting the negative values of $g(t)$ to be 0, in which case the local optima in the quantum control landscape are usually not global optima.

III. GLOBAL OPTIMIZATION

We employ two evolutionary computation techniques, the CMA-ES and SaDE, as global optimization methods. We compare the CMA-ES with the SaDE for three systems: (i) a mixture of three ^{6}Li atoms with two different hyperfine states ($N_\uparrow = 1$, $N_\downarrow = 2$, $\mu = 1$); (ii) a mixture of one ^{40}K atom and two ^{6}Li atoms ($N_\uparrow = 1$, $N_\downarrow = 2$, $\mu = 40/6$); and (iii) a mixture of two ^{40}K atoms and one ^{6}Li atom ($N_\uparrow = 2$, $N_\downarrow = 1$, $\mu = 40/6$). We numerically estimate the duration T_{QSL} for which the fidelity $F(T_{\mathrm{QSL}}) = 0.99$. We then compare the control field $g(t)$ for various durations T and depict the deviations between the optimized control field and nonoptimal ones. For simplicity, we present results on the 1K-2Li system unless stated otherwise.

The CMA-ES and SaDE are variants of the evolution strategy (ES) and DE, respectively. Both the ES and DE belong to the class of evolutionary algorithms and are stochastic, derivative-free algorithms for global optimization of fitness functions. An evolutionary algorithm works through a loop of variations (including recombination and mutation) and selection in each iteration (also called generation). New candidates are generated by variation of current parent individuals in each iteration. Then some candidates are selected, based on their fitness, to be parents for the next generation. In this way, search points with better and better values of the fitness function are generated over the sequence of iterations.

In the CMA-ES, new search points (parameter vectors) are sampled according to a multivariate normal distribution in the parameter space. The CMA-ES begins with a randomly initiated population of search points in the parameter space with the initial mean and covariant matrix. The population size N_p is the number of search points in each iteration. In the selection and recombination step, the search points with the best m fitness, where m is the parent size and not larger than the population size, are chosen as the parents to update the new mean, step-size, and covariant matrix. Recombination amounts to selecting a new mean value for the multivariate normal distribution. In the mutation step, the parameter vectors are further added by random vectors with zero mean and updated covariance matrix. The fitness function evolves iteratively towards its optimal state. In contrast to most other evolutionary algorithms, the CMA-ES is quasi-parameter-free: one needs only to randomly choose an initial value of the step size. In addition, the population size N_p does not depend on the dimension of the parameter space and can hence be chosen freely (which is in contrast to the DE). In general, large population sizes help to circumvent local optima, while small population sizes usually lead to faster convergence. Therefore, the trade-off between the computational cost and the performance needs to be carefully determined if the computational time for each iteration is considerably long. See [29] for a review of the CMA-ES method.

In Table I we list the values of fidelity for various combinations of N_c and N_p of duration $T = 0.1$ obtained using the CMA-ES method for the 1K-2Li system. The maximal fidelity in Table I is $F = 0.605\,37$ with ($N_c = 15$, $N_p = 60$). It is hardly possible to infer the optimal combination (N_c, N_p) to obtain the maximal fidelity for arbitrary durations or reasonable to try all possible combinations of (N_c, N_p), as the

TABLE I. Fidelity for various combinations of cutoff number N_c and population size N_p of duration $T = 0.1$ using the CMA-ES method for a 1K-2Li system. The maximal fidelity value is indicated by boldface font, and the corresponding pair of values is $N_c = 15$ and $N_p = 60$, respectively.

	N_c			
N_p	5	10	15	20
20	0.5995	0.5869	0.5933	0.5857
40	0.6021	0.5984	0.5924	0.5848
60	0.5968	0.6015	**0.6053**	0.5940
80	0.5963	0.5972	0.5987	0.5894

computational cost is huge. Therefore we fix the population size to $N_p^{\mathrm{ES}} = 60$ and the cutoff number of the Fourier basis $N_c = 15$ for all durations in the three few-fermion systems.

In the SaDE, an initial population of parameter vectors (called genome or chromosome) is randomly sampled. Then the mutant chromosomes are obtained from the differential mutation operation (origin of the term "DE"). In the mutation step, three mutually exclusive parameter vectors are generated randomly. The new set of parameter vectors is generated by adding one of these three vectors to the difference between the other two vectors with the mutation scale factor S, which controls the differential variation. In the recombination step, an offspring is formed by recombining the original and these mutant chromosome in a stochastic way, where the crossover rate Cr controls the probability of recombination. In the selection step, comparison of values of the fitness function determines whether the offspring or the original chromosome survives to the next generation. See Ref. [63] for a review of DE.

In the conventional DE algorithm, there are two free parameters, S, Cr, which are fixed through the iterations. In SaDE, however, S and Cr are adapted in each iteration to enhance the convergence rate for the high-dimensional optimization problem and to obtain better-quality solutions more efficiently, compared with the conventional DE. A reasonable value of N_p for the DE and its variants is usually chosen between $5D$ and $10D$ ($D = 3N_c$ is the dimension of the parameter space), as suggested in the field of evolutionary computation science [62]. Note, however, that this has not been tested in great detail for physically motivated quantum systems. In this work, we fix the population size $N_p = 5D$ and set the cutoff number to $N_c = 5$, thus $N_p^{\mathrm{DE}} = 75$, for the SaDE to reduce the computational cost. Details of the SaDE can be found in [26] and [27].

IV. RESULTS

First, we numerically compute the fidelity obtained for optimized and nonoptimal control fields, when the duration T of the time evolution is fixed to a certain value. We use the constraint that the interactions must be nonnegative at all times. We consider two typical nonoptimal rampings: linear ramping and exponential ramping. The latter is described by

$$g(t) = g_{\max}\frac{1 - e^{t/\tau}}{1 - e^{T/\tau}}, \tag{4}$$

where $\tau = T/5$. (In [17], the exponential ramping with particular values of T and τ is representative of quasiadiabatic ramping of the lattice depth used in experiments on optical lattices.) In Fig. 2, we take the 1K-2Li system and compare the fidelity (as a function of the duration) for the optimized ramping obtained using the CMA-ES method with that for exponential ramping and linear ramping. The shortest duration with fidelity $F = 0.99$ is $T_{\mathrm{Exp}} = 6.5$ for exponential ramping and $T_{\mathrm{Lin}} = 11$ for linear ramping, whereas $T_{\mathrm{Opt}} = 2.7$ for optimized ramping (note that the time unit is $1/\omega$). Thus the shortest duration obtained by the optimized control is approximately one-fourth of that using linear ramping, and two-fifths of that using exponential ramping, in the 1K-2Li system. This means that by controlling the interaction in the optimized way, one can significantly reduce the time for preparation of the system in the strongly correlated state.

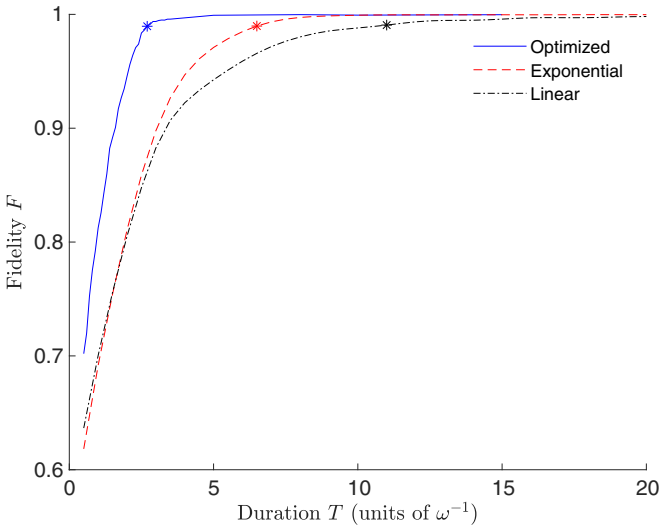

FIG. 2. Fidelity versus duration for the 1K-2Li system using different control fields: optimized (solid blue line), exponential (dashed red line), and linear (dash-dotted black line). The curve for the optimized control field is obtained using the CMA-ES algorithm. The stars mark the shortest durations for which a fidelity of $F = 0.99$ is reached: $T_{\mathrm{Opt}} = 2.7$, $T_{\mathrm{Exp}} = 6.5$, and $T_{\mathrm{Lin}} = 11$ (the time unit is ω^{-1}).

In Fig. 3, we show the optimized control field and the control fields of linear ramping and exponential ramping for different durations. For a very short duration ($T = 0.5$), the optimized control field shows a few large oscillations, while $g(t)$ remains 0 for most of the time. [Note the requirement that $g(t) \geqslant 0$]. As the duration approaches $T_{\mathrm{Opt}} = 2.7$, which is an estimate of the quantum speed limit $T \approx T_{\mathrm{QSL}}$ [Fig. 3(b)], more oscillations emerge to make the transformation as fast as possible and the fidelity as high as possible. The deviation between the

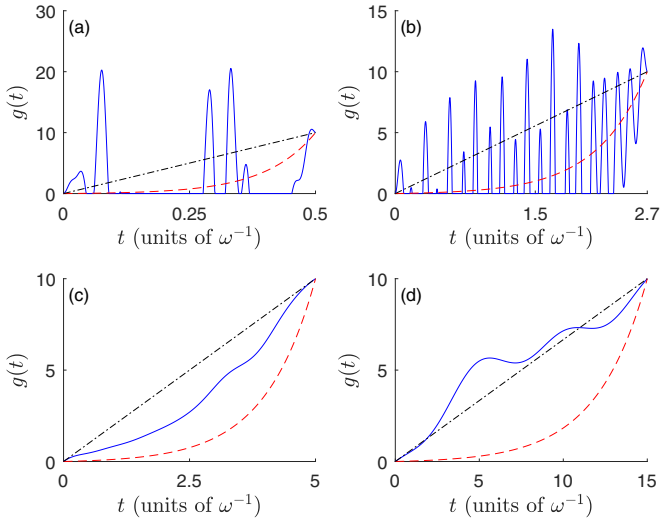

FIG. 3. Control field for different durations in a 1K-2Li system. (a) $T = 0.5$, (b) $T = 2.7$, (c) $T = 5$, and (d) $T = 15$ (the time unit is ω^{-1}). Solid blue lines are the optimized control fields obtained using the CMA-ES method; dashed red lines, exponential rampings; and dash-dotted black lines, linear rampings.

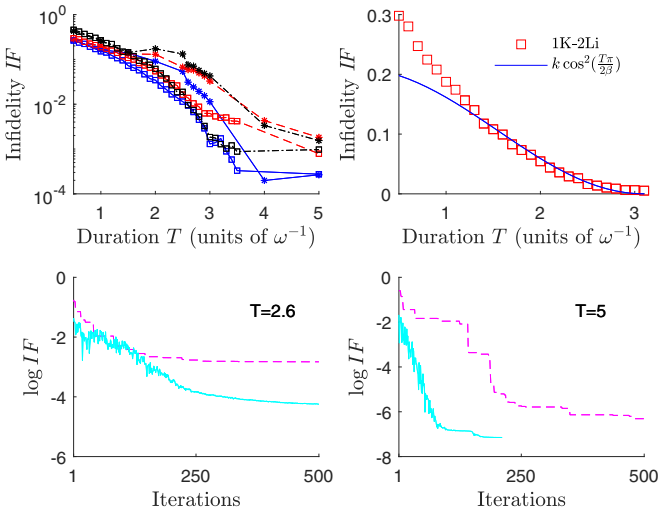

FIG. 4. Comparing the CMA-ES and SaDE. Top left: The infidelity (IF $= 1 - F$) as a function of the duration T using the CMA-ES (squares) and SaDE (asterisks) for 1Li-2Li (solid blue line), 1K-2Li (dashed red line), and 2K-1Li (dash-dotted black line), where the vertical axis is on the logarithm scale. Top right: Red squares represent numerical data, which are obtained using the CMA-ES method, for the infidelity IF as a function of the duration T for the 1K-2Li system, while solid blue lines show the fitting obtained using the function $k\cos^2(\frac{T\pi}{2\beta})$ for the numerical results, where k and β are free fitting parameters. Bottom: Comparisons of log-infidelity versus iterations in the 1K-2Li system are shown between the CMA-ES (solid cyan line) and the SaDE (dashed magenta line) for durations $T = 2.6$ (bottom left) and $T = 5$ (bottom right), with the time unit ω^{-1}.

optimized control field and the linear and exponential ones is thus large for such durations. When the duration is much larger than $T_{\rm Opt}$, e.g., $T = 5$ [Fig. 3(c)] and $T = 15$ [Fig. 3(d)], the highly oscillating components are no longer necessary and the deviations between different rampings are much smaller than in the cases in which $T < T_{\rm Opt}$. Also, the fidelities at the longer durations do not depend that much on the way we approach the strong interaction. This observation means that for long enough times, the exact shape of the control field does not matter. This is why slow enough processes are quasiadiabatic and the quantum state can be transferred when carefully managed. Since we require the interaction strength to be nonnegative, $g \geqslant 0$, the lower bound of the control field is 0, but there is no upper bound. As mentioned above, if $g(t)$ [as given in Eq. (3)] is negative in some time interval, we put $g(t)$ equal to 0 in that interval, as shown in Fig. 3. Such processes introduce the possibility of sharp peaks in the control fields and thereby high Fourier components. Given the particular experimental constraints of the system, one may perform an analog optimization with appropriate constraints included.

The comparisons between CMA-ES and SaDE for three few-fermion systems are shown in Fig. 4. To reduce the computational cost, we set the maximal number of iterations to 500. In addition, we set up halt criteria for the CMA-ES and SaDE methods. For both of them, the calculations stop if the distance between the minimal and the maximal fidelity in the population is smaller than a threshold value (Error $= 10^{-6}$). The top-left panel depicts the infidelity $IF = 1 - F$ as a function of the duration T for three systems using the CMA-ES and SaDE methods. For short durations, $T < 1.5$, the infidelities obtained using the CMA-ES and SaDE are very close. For long durations, $T > 1.5$, however, the infidelities obtained with the CMA-ES are smaller than those with the SaDE (apart from $T = 4$ for the 1Li-2Li system), which means that the performance of the CMA-ES is better than that of the SaDE in terms of the best infidelity with the specific parameters (N_p, N_c) used for both global optimization methods in this work. It is noteworthy that the estimate of the QSL is approximately proportional to the inverse of the energy gap, i.e., $T_{\rm QSL} \sim \pi/\Delta$, where $\Delta \approx 1$ is the energy gap to the nearest coupled excited state for all three few-fermion systems (see Fig. 1). This fact agrees with the conclusion obtained in Ref. [21]. In the top-right panel, we show the numerical results for the infidelity IF as a function of the duration T for the 1K-2Li system using the CMA-ES method and the curve fitting using the cosine square function $k\cos^2(\frac{T\pi}{2\beta})$ with two free fitting parameters (k, β). The single cosine square function does not fit well for the numerical results. Such deviations or discrepancies are also found in different quantum systems [13,18,64].

In the bottom panel in Fig. 4, we demonstrate the log-infidelity versus iterations (also called generation in evolutionary computation) for durations $T = 2.6$ (bottom left) and $T = 5$ (bottom right) in the 1K-2Li system. We observe that the log-infidelity starts to converge after a certain number of iterations (several tens to several hundreds) in the CMA-ES method, while a "staircase" pattern emerges in most cases with the SaDE method. From the lower panel in Fig. 4, the CMA-ES method performs better than the SaDE method in terms of the best infidelity and convergence rate. The reason why the CMA-ES performs better than the SaDE might be that the cutoff number of the Fourier basis of the CMA-ES, $N_c^{\rm ES} = 15$, is larger than that of the SaDE, $N_c^{\rm DE} = 5$, such that the search space of the CMA-ES is larger than that of the SaDE. Note, however, that the population size of the CMA-ES ($N_p^{\rm ES} = 60$) is smaller than that of the SaDE ($N_p^{\rm DE} = 75$).

Since the numerical calculations studied in this work are considerably time-consuming, the convergence rate of the optimization method is one of the most important considerations. Therefore, the CMA-ES is preferable to the SaDE because the CMA-ES does not require the use a large population size [29]. When the computational cost is low, the primary consideration is whether a satisfactory result, e.g., a certain threshold value of the fitness function, is achieved by the optimization method [25].

From the experimental point of view a very important question arises: How sensitive is the final fidelity with respect to small changes in the optimal control field? To demonstrate the robustness of the optimized control field obtained using global optimization methods, we depict in Fig. 5 comparisons between optimized control fields and the corresponding modification for the durations $T = 2.6$ and $T = 5$. The modified optimized control fields are obtained by mixing the optimized control field and linear ramping with different values of weight $w \in [0.1, 0.9]$, i.e., $g(t) = wg_{\rm Lin}(t) + (1 - w)g_{\rm Opt}(t)$. As shown in the top panel in Fig. 5, the differences between the fidelity of the optimized control field $F_{\rm o}$ and that of the modification $F_{\rm w}$ increases as the weight of linear ramping

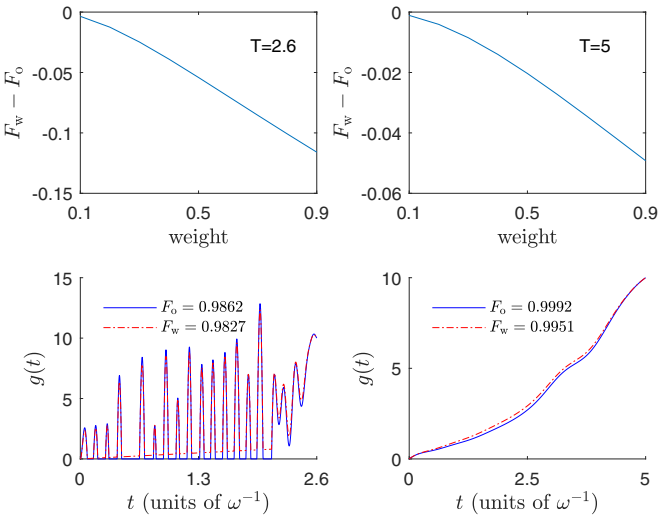

FIG. 5. Effects of deviations from the optimized control fields, which are obtained by mixing the optimized control field and linear ramping with a certain weight. Top: The deviation between the fidelity of the modified optimized control field F_w and that of the optimized control field F_o are shown as a function of the weight for $T = 2.6$ (left) and $T = 5$ (right), with the time unit ω^{-1}. Bottom: Both the optimized control field (solid blue line) and its modification whose weight is 10% (dash-dotted red line) are shown for $T = 2.6$ (left) and $T = 5$ (right). The fidelity of the optimized control field F_o and that of the modified one F_w are also shown, and the difference between them is of order 10^{-3} for both durations.

grows (note that $F_w < F_o$). For a special case where the weight is 10%, as shown in the bottom panel in Fig. 5, the differences between the fidelities are of order 10^{-3} for $T = 2.6$ and $T = 5$. This means that the optimized control fields obtained are robust to the imperfection or external noise which is naturally present in experiments. Thus, the scheme may be especially relevant in future experiments.

V. DISCUSSION

As two of the most promising evolutionary algorithms, the CMA-ES method and the SaDE method outperform other evolutionary computational algorithms and local optimization algorithms for high-dimensional optimization problems in certain quantum systems [28,29,63]. Both algorithms, however, have their own advantages and disadvantages, and the preferences may vary from one case to another. The CMA-ES method is quasi-parameter-free, while the SaDE method requires the user to determine more initial parameters. For the SaDE method, as mentioned in Sec. III, the population size N_p is fixed to be $5D$, which is suggested as a lower bound and has been tested in great detail in the field of computational science (but not as extensively for physically motivated quantum systems). For the CMA-ES method, there is no guide for choosing the value of N_p, thus we choose $N_p = 60$, which is large enough to guarantee that the fidelity is saturated. Therefore, in general, the population size of SaDE is larger than that of CMA-ES, especially in high-dimension parameter space, thus the computational time of the SaDE is longer than that of the CMA-ES. As for the convergence rate, in general, the CMA-ES converges more rapidly than the SaDE. The slow convergence of the SaDE is depicted in Fig. 4 (bottom right), where the width of the staircase indicates the stagnation of the SaDE method. Note, however, if the N_c of the SaDE is the same as that of the CMA-ES, the final fidelity obtained using the SaDE method is generally higher than that using the CMA-ES method, though the computational time of the SaDE is much longer than that of the CMA-ES. For instance, suppose that ($N_c = 15, N_p = 5D$) is taken for the SaDE method, which is the same as for the CMA-ES; then the computational time of the SaDE is approximately three times longer than that of the CMA-ES.

The calculations are performed in parallel using MATLAB R2017a on cluster (Intel Xeon E5-2680 CPU with 28 cores and 251 GB RAM). Take the CMA-ES, for instance; the computational time of the CMA-ES method over 500 iterations is about 31 h for $T = 1.5$ and 71 h for $T = 2.5$. For the same process duration T and number of iterations, the computational time ratio of CMA-ES to SaDE is roughly 60:75, which is the ratio of the population size. This is because the maximal number of cores in the cluster is 28. If the number of cores is larger than the population size, then the computational time ratio of CMA-ES to SaDE is approximately 1:1.

VI. CONCLUSION

We have given numerical estimates of the quantum speed limit for three few-fermion systems confined in a one-dimensional harmonic trap using the CMA-ES and the SaDE methods and shown that the shortest duration obtained employing optimized, nonadiabatic processes is much faster than in the case of linear ramping and exponential ramping. One can achieve at least double speedup in obtaining the target three-body ground state by using our optimized approach compared to exponential ramping (see Fig. 2). Since the Hilbert space increases greatly with the number of particles, the speedup might increase even further for systems with more than three particles. We observed that for durations shorter than the estimate of the quantum speed limit the optimized fields are of the oscillation type, while for longer times, the optimized fields do not change drastically over time, which is analogous to the linear ramping and the exponential ramping. We have compared the performance of the CMA-ES and the SaDE methods and found that the performance of the CMA-ES is better than that of the SaDE in terms of the best infidelity and convergence rate for the parameters considered in this paper. In addition, we have explained the advantages and disadvantages of the CMA-ES method, as well as the SaDE method, and the preference varies from one case to another. Moreover, we have also demonstrated the robustness of the optimized control field to minor variations. This stability of the above scheme to small variations led us to believe that the obtained optimized fields are not just a purely numerical prediction but can be useful in the noisy laboratory environment.

The present work shows the encouraging result that control theory can be used to obtain a significant speedup in producing a target state with the same symmetry as the initial state. As the next step, it would be very interesting to investigate how one can design control protocols to produce any of the low-energy

states in the spectrum with a high fidelity starting from the ground state of the noninteracting system.

ACKNOWLEDGMENTS

We would like to thank Nikolaj T. Zinner for discussions. This work was supported in part by the Villum Foundation. D.P. and T.S. acknowledge support from (Polish) National Science Center Grants No. 2016/21/N/ST2/03315 (D.P.) and No. 2016/22/E/ST2/00555 (T.S.). J.S. acknowledges support from ERC. X.L. thanks the Max Planck Institute for the Physics of Complex Systems for hospitality during visits to the institute.

[1] D. D'Alessandro, *Introduction to Quantum Control and Dynamics* (Chapman & Hall/CRC, Boca Raton, FL, 2007).
[2] C. Brif, R. Chakrabarti, and H. Rabitz, New J. Phys. **12**, 075008 (2010).
[3] V. F. Krotov, *Global Methods in Optimal Control Theory* (Marcel Dekker, New York, 1996).
[4] T. Gericke, F. Gerbier, A. Widera, S. Fölling, O. Mandel, and I. Bloch, J. Mod. Opt. **54**, 735 (2007).
[5] R. Modak, L. Vidmar, and M. Rigol, Phys. Rev. E **96**, 042155 (2017).
[6] S. Deng, P. Diao, Q. Yu, A. del Campo, and H. Wu, Phys. Rev. A **97**, 013628 (2018).
[7] L. Mandelshtam and Ig. Tamm, J. Phys. (USSR) **9**, 249 (1945).
[8] M. Gajdacz, K. K. Das, J. Arlt, J. F. Sherson, and T. Opatrný, Phys. Rev. A **92**, 062106 (2015).
[9] L. B. Levitin and T. Toffoli, Phys. Rev. Lett. **103**, 160502 (2009).
[10] S. Deffner and E. Lutz, Phys. Rev. Lett. **111**, 010402 (2013).
[11] A. del Campo, I. L. Egusquiza, M. B. Plenio, and S. F. Huelga, Phys. Rev. Lett. **110**, 050403 (2013).
[12] M. G. Bason *et al.*, Nat. Phys. **8**, 147 (2012).
[13] J. J. W. H. Sørensen *et al.*, Nature **532**, 210 (2016).
[14] S. Lloyd and S. Montangero, Phys. Rev. Lett. **113**, 010502 (2014).
[15] S. J. Glaser *et al.*, Eur. Phys. J. D **69**, 279 (2015).
[16] P. Doria, T. Calarco, and S. Montangero, Phys. Rev. Lett. **106**, 190501 (2011).
[17] S. Rosi, A. Bernard, N. Fabbri, L. Fallani, C. Fort, M. Inguscio, T. Calarco, and S. Montangero, Phys. Rev. A **88**, 021601(R) (2013).
[18] S. van Frank *et al.*, Sci. Rep. **6**, 34187 (2016).
[19] T. Caneva, T. Calarco, and S. Montangero, New J. Phys. **14**, 093041 (2012).
[20] D. Burgarth, K. Maruyama, M. Murphy, S. Montangero, T. Calarco, F. Nori, and M. B. Plenio, Phys. Rev. A **81**, 040303(R) (2010).
[21] T. Caneva, T. Calarco, and S. Montangero, Phys. Rev. A **84**, 022326 (2011).
[22] S. E. Sklarz and D. J. Tannor, Phys. Rev. A **66**, 053619 (2002).
[23] N. Khaneja, T. Reiss, C. Kehlet, T. Schulte-Herbrüggen, and S. J. Glaser, J. Magn. Reson. **172**, 296 (2005).
[24] S. Machnes, D. J. Tannor, F. K. Wilhelm, and E. Assémat, arXiv:1507.04261.
[25] E. Zahedinejad, S. Schirmer, and B. C. Sanders, Phys. Rev. A **90**, 032310 (2014).
[26] P. Palittapongarnpim, P. Wittek, E. Zahedinejad, S. Vedaie, and B. C. Sanders, Neurocomputing **268**, 116 (2017).
[27] J. Brest, S. Greiner, B. Bošković, M. Mernik, and V. Žumer, IEEE Trans. Evol. Comput. **10**, 646 (2006).
[28] O. M. Shir, J. Roslund, D. Whitley, and H. Rabitz, arXiv:1112.4454.
[29] N. Hansen, in *Towards a New Evolutionary Computation. Advances in Estimation of Distribution Algorithms* (Springer, Berlin, 2006), pp. 75–102.
[30] J. J. W. H. Sørensen, M. Aranburu, T. Heinzel, and J. Sherson, arXiv:1802.07521.
[31] H. A. Rabitz, M. Hsieh, and C. M. Rosenthal, Science **303**, 1998 (2004).
[32] B. Paredes, A. Widera, V. Murg, O. Mandel, S. Fölling, I. Cirac, G. V. Shlyapnikov, T. W. Hänsch, and I. Bloch, Nature **429**, 277 (2004).
[33] T. Kinoshita, T. Wenger, and D. S. Weiss, Science **305**, 1125 (2004).
[34] E. Haller, M. Gustavsson, M. J. Mark, J. G. Danzl, R. Hart, G. Pupillo, and H. C. Nägerl, Science **325**, 1224 (2009).
[35] F. Serwane, G. Zürn, T. Lompe, T. B. Ottenstein, A. N. Wenz, and S. Jochim, Science **332**, 336 (2011).
[36] G. Zürn, F. Serwane, T. Lompe, A. N. Wenz, M. G. Ries, J. E. Bohn, and S. Jochim, Phys. Rev. Lett. **108**, 075303 (2012).
[37] G. Zürn, A. N. Wenz, S. Murmann, A. Bergschneider, T. Lompe, and S. Jochim, Phys. Rev. Lett. **111**, 175302 (2013).
[38] A. N. Wenz, G. Zürn, S. Murmann, I. Brouzos, T. Lompe, and S. Jochim, Science **342**, 457 (2013).
[39] S. Murmann, A. Bergschneider, V. M. Klinkhamer, G. Zürn, T. Lompe, and S. Jochim, Phys. Rev. Lett. **114**, 080402 (2015).
[40] S. Murmann, F. Deuretzbacher, G. Zürn, J. Bjerlin, S. M. Reimann, L. Santos, T. Lompe, and S. Jochim, Phys. Rev. Lett. **115**, 215301 (2015).
[41] A. M. Kaufman, B. J. Lester, M. Foss-Feig, M. L. Wall, A. M. Rey, and C. A. Regal, Nature **527**, 208 (2015).
[42] T. Sowiński, M. Gajda, and K. Rzażewski, Europhys. Lett. **109**, 26005 (2015).
[43] E. J. Lindgren, J. Rotureau, C. Forssén, A. G. Volosniev, and N. T. Zinner, New J. Phys. **16**, 063003 (2014).
[44] P. D'Amico and M. Rontani, Phys. Rev. A **91**, 043610 (2015).
[45] S. E. Gharashi and D. Blume, Phys. Rev. Lett. **111**, 045302 (2013).
[46] T. Grining, M. Tomza, M. Lesiuk, M. Przybytek, M. Musial, P. Massignan, M. Lewenstein, and R. Moszynski, New J. Phys. **17**, 115001 (2015).
[47] J. Decamp, P. Armagnat, B. Fang, M. Albert, A. Minguzzi, and P. Vignolo, New J. Phys. **18**, 055011 (2016).
[48] F. Deuretzbacher, D. Becker, J. Bjerlin, S. M. Reimann, and L. Santos, Phys. Rev. A **90**, 013611 (2014).
[49] L. Yang, L. Guan, and H. Pu, Phys. Rev. A **91**, 043634 (2015).
[50] L. Yang and X. Cui, Phys. Rev. A **93**, 013617 (2016).

[51] E. Wille, F. M. Spiegelhalder, G. Kerner, D. Naik, A. Trenkwalder, G. Hendl, F. Schreck, R. Grimm, T. G. Tiecke, J. T. M. Walraven, S. J. J. M. F. Kokkelmans, E. Tiesinga, and P. S. Julienne, Phys. Rev. Lett. **100**, 053201 (2008).
[52] T. G. Tiecke, M. R. Goosen, A. Ludewig, S. D. Gensemer, S. Kraft, S. J. J. M. F. Kokkelmans, and J. T. M. Walraven, Phys. Rev. Lett. **104**, 053202 (2010).
[53] M. Cetina, M. Jag, R. S. Lous, I. Fritsche, J. T. M. Walraven, R. Grimm, J. Levinsen, M. M. Parish, R. Schmidt, M. Knap, and E. Demler, Science **354**, 96 (2016).
[54] D. Pęcak, M. Gajda, and T. Sowiński, New J. Phys. **18**, 013030 (2016).
[55] D. Pęcak, and T. Sowiński, Phys. Rev. A **94**, 042118 (2016).
[56] D. Pęcak, M. Gajda, and T. Sowiński, Few-Body Syst. **58**, 159 (2017).
[57] M. A. García-March, A. S. Dehkharghani, and N. T. Zinner, J. Phys. B: At. Mol. Opt. Phys. **49**, 075303 (2016).
[58] N. J. S. Loft, A. S. Dehkharghani, N. P. Mehta, A. G. Volosniev, and N. T. Zinner, Eur. Phys. J. D **69**, 65 (2015).
[59] N. L. Harshman, M. Olshanii, A. S. Dehkharghani, A. G. Volosniev, S. G. Jackson, and N. T. Zinner, Phys. Rev. X **7**, 041001 (2017).
[60] A. G. Volosniev, Few-Body Syst. **58**, 54 (2017).
[61] M. Olshanii, Phys. Rev. Lett. **81**, 938 (1998).
[62] R. Storn and K. V. Price, J. Global Optimizat. **11**, 341 (1997).
[63] S. Das and P. N. Suganthan, IEEE Trans. Evol. Comput. **15**, 4 (2011).
[64] M. Bukov *et al.*, arXiv:1705.00565v2.